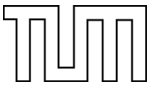

Technische Universität München

Department of Mathematics

Bachelor's Thesis

Reduction of limited-angle artifacts in computed tomography

Thomas Obermüller

Supervisor: Prof. Dr. Rupert Lasser

Advisor: Dr. Laurent Demaret

Submission Date: 26.04.2013

I assure the single handed composition of this bachelor's thesis only supported by declared resources.

Garching,

Zusammenfassung

Thema dieser Bachelorarbeit ist die Computertomographie. In der Computertomographie versucht man Informationen über das Innere eines Objekts aus einer Vielzahl seiner Projektionen zu gewinnen. Die Computertomographie ist der Prototyp eines inversen Problems und bedingt durch seine vielfältigen Anwendungsmöglichkeiten in der industriellen und medizinischen Bildgebung wurde in den letzten Jahrzehnten stark an der Stabilisierung der zugrundeliegenden Rekonstruktionsalgorithmen gearbeitet.

Diese Arbeit befasst sich genauer mit dem Problem der Tomographie unter eingeschränktem Winkelbereich, welches sich aus verschiedenen Anwendungen in der industriellen und medizinischen Bildgebung ergibt. In diesen Anwendungen ist der mögliche Winkelbereich beschränkt, so dass Tomographie-Daten in einem zusammenhängenden Winkelbereich fehlen. Als Folge dessen ist das betrachtete Rekonstruktionsproblem enorm schlecht gestellt und charakteristische Bildartefakte entstehen in den berechneten Bildern.

Unser Ziel ist es eine Methode zu entwickeln, welche diese Artefakte reduziert und dabei so viel Information wie möglich aus den gegebenen Daten nutzt. über den Verlauf dieser Arbeit werden wir zwei Methoden vorstellen, welche gegebene Tomographie-Daten geeignet für eine weitere Verarbeitung mit einer herkömmlichen Rekonstruktionsmethode aufbereiten. Davor machen wir uns mit der Computertomographie, der ihr zugrundeliegenden Mathematik und der Rekonstruktion durch gefilterte Rückprojektion vertraut.

In unserem ersten Ansatz verwenden wir eine starke Modellannahme, indem wir davon ausgehen, dass unser untersuchtes Objekt aus einer Superposition von einer oder mehreren Ellipsen besteht. Dies ermöglicht es uns Tomographie-Daten über den gesamten Winkelbereich wiederherzustellen, was insbesondere durch die Ludwig-Helgason Konsistenzbedingungen motiviert wird. Nur bei Erfüllung dieser Bedingungen können Tomographie-Daten im Bild der Radon-Transformation liegen. Die Radon Transformation ist der mathematische Operator, welcher die Computertomographie modelliert.

Ausgehend von den im ersten Ansatz gewonnenen Kenntnissen, leiten wir eine weitere Methode her, welche die Daten nur in einer lokalen Nachbarschaft am Rand der verfügbaren Daten wiederherstellt. Das Ziel dieser Strategie ist es die durch den eingeschränkten Winkelbereich hervorgerufenen Artefakte zu reduzieren und dabei sowohl so viel Information wie möglich aus den gegebenen Daten zu verarbeiten, als auch so wenig neue Information wie möglich hinzuzufügen. Unser Vorgehen bei diesem Ansatz basiert auf Ergebnissen aus dem Gebiet der mikrolokalen Tomographie, welches wir kurz einführen werden.

Contents

1 Introduction

The main topic of this bachelor's thesis is computerized tomography. In computerized tomography one generally wants to gain knowledge about the interior of an object from a number of its projections. It is the prototype of an inverse problem and since it has various applications in industrial and medical imaging, a lot of effort has been made in stabilization of underlying reconstruction algorithms during past decades.

To be more specific, we are concerned with the problem of *limited angle tomography* that arises naturally from various medical and industrial applications. These applications enforce a limitation on the angular range of tomographic data so that a coherent range of angles is missing in tomography data. As a consequence we have to deal with a severely ill-posed reconstruction problem, in which certain artifacts are produced in reconstructed images.

In the following it is our goal to find a method which reduces these artifacts, while still incorporating as much information from the limited angle data as possible. We have come upon two methods acting on projection data ("sinogram") during research. These methods shall be derived and evaluated over the course of this thesis. Before that, we start of by familiarizing ourselfs with computed tomography, its underlying mathematics, and the filtered backprojection reconstruction method.

In our first approach we employ a strong model requirement. We assume that the object examined is a superposition of one or more ellipses. This enables us to recover data for the full range of projections, which is motivated by the so called Ludwig-Helgason consistency conditions. Fulfillment of these conditions is required for tomographic data to lie in the range of the Radon transform - the mathematical operator modelling computed tomography.

We use the knowledge gained in our first approach to derive a second method that restores information in a local neighbourhood of missing data. The aim of our strategy is to reduce artifacts inherent to the limited angle problem, while keeping as much information as possible from available projections and adding as less new information as possible. Our procedure for this approach is motivated by results of microlocal tomography, which we will briefly introduce.

I have to express my profoundest gratitude to my thesis adviser, Dr. Laurent Demaret. He gave me great freedom in writing this thesis and still pointed out a direction, whenever this was necessary. Without his patience and constant encouragement throughout the last month, this thesis would not have been possible to accomplish. Furthermore I would like to express my sincere gratitude to Prof. Dr. Rupert Lasser, who agreed to be supervisor for this thesis.

2 Basic properties of the limited angle tomography problem

In this chapter we present basic concepts and properties of the limited angle tomography problem. We begin with an overview of modern computerized tomography, introduce the Radon transform and present the method of tomographic reconstruction through filtered backprojection. Lastly we state the limited angle problem, which we want to consider throughout this thesis.

Mathematics of computerized tomography are understood quite well and numerous articles and books have been published on the subject. In our discussion over the course of this chapter we aggregate some well known results that can be found in the textbooks [Nat01, NW01, RK96, Eps08], to which we refer the keen reader for further information and proof of given theorems.

2.1 Overview of computerized tomography

The word tomography is derived from the Greek words tome ("cut") and graphein ("to write"). It is a broader term for various methods in medical imaging that allow the reconstruction of an objects' unknown interior from a number of one dimensional projections. The great advantage of these methods, in contrast to conventional x-ray projection, is that they produce superposition free slices of the examined object.

Common examples for tomographic methods are computed tomography (CT), single-photon emission computed tomography (SPECT), magnetic resonance imaging (MRI) or positron emission tomography (PET). They are used in a variety of medical and industrial applications, which led to an increased interest for an efficient implementation of the underlying algorithms during the past decades.

This bachelor's thesis is concerned with classical x-ray computed tomography using parallel beam geometry. In a modern computer tomograph data is obtained by rotating an emitter and a set of detectors around the object of interest, while it gathers the attenuation of penetrating rays at evenly spaced angles. The so gained projection data serves as input for a tomographic reconstruction software that produces an image of the objects' interior.

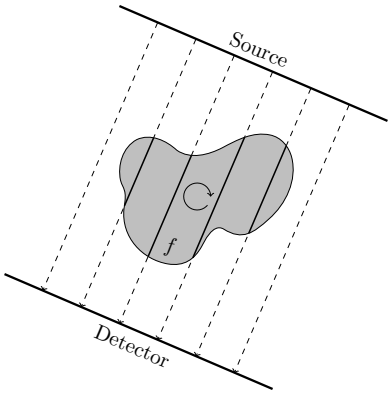

Figure 1 – The mechanism of computed tomography: Opposing arrays of emitters and detectors are rotated around the object of interest. Rays penetrating the object are attenuated and consequently the distribution of the attenuation coefficient is gathered for evenly-spaced angles. Projection data is then used to reconstruct the objects' interior.

2.2 Mathematical notation and definitions

Before we can start to introduce the mathematics of computed tomography, let us first provide definitions and notations for some objects that we will come across frequently throughout this thesis. As computed tomography is a rich subject, various tools out of the mathematical toolbox are required. To begin with, let us recall the notation of a few classical function spaces:

$C^\infty(U)$	(space of smooth functions)
$L^p(U)$	(space of p-integrable functions)
$L^p(U, d\mu)$	(space of weighted p-integrable functions).

A function space that is particularly important for the Fourier and Radon transform is the Schwartz space $\mathcal{S}(\mathbb{R}^n)$. It consists of all infinitely differentiable functions $f(x) \in C^\infty(\mathbb{R}^n)$ which rapidly decay with all their derivatives; or more precisely $f \in \mathcal{S}(\mathbb{R}^n)$ if, and only if

$$\sup_{x \in \mathbb{R}^n} \left| x^\alpha \partial_x^\beta f(x) \right| < \infty,$$

where $\partial_x = (\frac{\partial}{\partial x_1}, \ldots, \frac{\partial}{\partial x_n})$ and $\alpha, \beta \in \mathbb{N}_0^n$ are arbitrary multi-indices (tuples of non-negative integers). Let us now define several important sets that we will use.

$B_r^n := \{x \in \mathbb{R}^n : \|x\|_2 \leq r\}, \quad r \in \mathbb{R}^+$	(ball with radius r in $\mathbb{R}^n$)
$S^{n-1} := \{x \in \mathbb{R}^n : \|x\|_2 = 1\}$	(unit sphere in $\mathbb{R}^n$)
$Z^n := S^{n-1} \times \mathbb{R}$	(unit cylinder in $\mathbb{R}^n$)
$L(\theta, t) := \{x \in \mathbb{R}^n : x \cdot \theta = t\}, \quad \theta \in \mathbb{R}^n, t \in \mathbb{R}$	(affine hyperplane in $\mathbb{R}^n$)

As we will later see, the Fourier transform is closely related to the Radon transform. For $f, g \in \mathcal{S}(\mathbb{R}^n)$, we use the following definitions for the Fourier transform $\mathcal{F}$ and its inverse $\mathcal{F}^{-1}$:

$$\hat{f}(\xi) := \mathcal{F}f(\xi) := \int_{\mathbb{R}^n} f(x) e^{ix \cdot \xi} dx,$$

$$f(x) = \mathcal{F}^{-1}\hat{f}(x) := \frac{1}{(2\pi)^n} \int_{\mathbb{R}^n} \hat{f}(\xi) e^{-ix \cdot \xi} d\xi.$$

We will also need the convolution in $\mathbb{R}^n$, which we define through

$$(f * g)(x) := \int_{\mathbb{R}^n} f(x - y) g(y) dy$$

for $f, g \in \mathcal{S}(\mathbb{R}^n)$. When f is a function of two variables, its convolution and Fourier transform are always taken with respect to the second variable throughout this bachelor's thesis. In the following sections we are going to proceed with definition and characterization of the Radon transform.

2.3 The Radon transform

Mathematical foundations of computerized tomography have been set in 1917 by Johann Radon in his writing "Über die Bestimmung von Funktionen durch ihre Integralwerte längs gewisser Mannigfaltigkeiten" [Rad17; translated in Rad86]. The publication shows that it is theoretically possible to recover a function f on $\mathbb{R}^2$ from its line integrals. Consequently the transform that maps a function of points to a function of plane integrals, became known as *Radon transform*. We are now going to introduce it.

Definition 2.1. The Radon transform $\mathcal{R}f : Z^n \to \mathbb{R}$ of a function f from n-dimensional Schwartz space $S(\mathbb{R}^n)$ is defined by

$$\tilde{f}(\theta, t) := \mathcal{R}f(\theta, t) := \int_{L(\theta,t)} f(x)dx, \tag{2.1}$$

where $L(\theta, t)$ is an affine hyperplane in $\mathbb{R}^n$ and dx is the associated Lebesgue measure. In the following we will sometimes write $\mathcal{R}_\theta f(t)$ for $\mathcal{R}f(\theta, t)$.

Figure 2 depicts the geometry of the Radon transform in a two dimensional setting: An unknown function f is integrated along lines orthogonal to the unit vector θ with a lateral displacement of t in direction θ. We identify the vector θ with an angle $\phi \in [0, 2\pi]$ by setting $\theta = (\cos\phi, \sin\phi)$ and note that integrating along a line $L(\theta, t)$ can be seen as attenuation of a ray through an object in the computer tomograph.

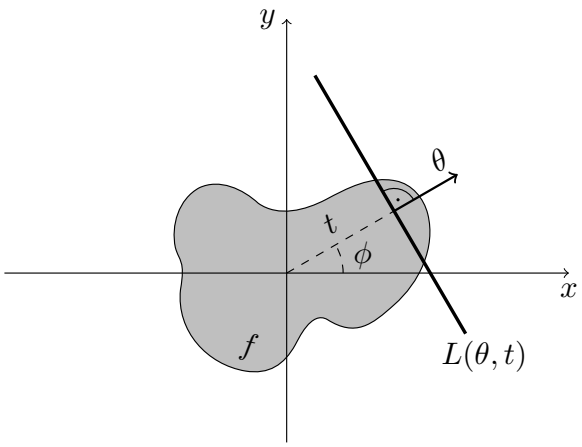

Figure 2 – The geometry of computed tomography: An unknown function $f \in \mathbb{R}^2$ is integrated over all lines $L(\theta, t)$ parametrized by the unit vector $\theta = (\cos\phi, \sin\phi)$, $\phi \in [0, 2\pi]$ and a lateral displacement $t \in \mathbb{R}$.

Remark. We have defined the Radon transform as an operator $\mathcal{R} : \mathcal{S}(\mathbb{R}^n) \to \mathcal{S}(Z^n)$. However it can also be introduced for or extended to some other spaces. It is important to note that the operator is unbounded on $L^2(\mathbb{R}^n)$, even though $S(\mathbb{R}^n)$ is dense in $L^2(\mathbb{R}^n)$. A key factor that the Radon transform of a function is well-behaved is if it has a compact support. For example it is shown in [Nat01, p. 17] that $\mathcal{R} : L_2(B_1^n) \to L_2(Z^n, (1 - s^2)^{(1-n)/2})$ is a continuous operator. We will assume that the Radon transform is defined for the objects used, yet one may find characterization of its domain in the textbooks mentioned in introduction of this chapter.

2.3.1 Basic properties of the Radon transform

Now that we have defined the Radon transform, let us aggregate some of its basic properties and well known statements.

Proposition 2.2 ([RK96, pp. 11-14])**.** *If $f, g \in \mathcal{S}(\mathbb{R}^n)$, $\theta \in \mathbb{R}^n$, $t \in \mathbb{R}$, then the following statements hold*

1. *$\mathcal{R}$ is a linear operator, $\mathcal{R}(af + g) = a\mathcal{R}(f) + \mathcal{R}(g)$.*
2. *$\mathcal{R}f$ is an even function, $\mathcal{R}f(\theta, t) = \mathcal{R}f(-\theta, -t)$.*
3. *If $f_\xi(x) := f(x + \xi)$, then $\mathcal{R}f_\xi(\theta, t) = \mathcal{R}f(\theta, t + \xi \cdot \theta)$.*

2.3.2 Radon transform of a convolution

As the next proposition states, convolution in $\mathbb{R}^n$ is converted to convolution in the affine parameter by the Radon transform. Note that $*$ on the right hand side of the equation indicates one-dimensional convolution with respect to the second argument of functions Rf and Rg here.

Proposition 2.3 ([NW01, Theorem 2.2]). *Assume $f, g \in \mathcal{S}(\mathbb{R}^n), \theta \in \mathbb{R}^n, t \in \mathbb{R}$. Then*

$$\mathcal{R}(f * g)(\theta, t) = \mathcal{R}f * \mathcal{R}g. \tag{2.2}$$

2.3.3 Fourier slice theorem

An important result for the Radon transform is its connection with the Fourier transform. The *Fourier slice theorem* states that it is equal to take the one-dimensional Fourier transform of a function's projection on a plane and to take a slice of the function's two-dimensional Fourier transform, whereby the slice has to be parallel to the projection and going through the origin. This theorem is sometimes also referred to as *projection slice theorem*.

Theorem 2.4 ([NW01, Theorem 2.1]). *For $f \in \mathcal{S}(\mathbb{R}^n)$ we have*

$$\widehat{\mathcal{R}_\theta f}(\sigma) = \hat{f}(\sigma\theta),\ \sigma \in \mathbb{R} \tag{2.3}$$

In computed tomography we are given data $\mathcal{R}f$ and want to draw conclusions about the transformed function f. In this manner we are now going to familiarize ourselfs with an inversion method for the Radon transform.

2.4 Inversion of the Radon transform

Reconstruction methods for tomographic data fall in two classes. Analytical methods which take a direct approach to the mathematical problem and algebraic methods that address a discrete version of the problem. The method of *filtered backprojection (FBP)* is an analytical method; it is often employed in practical settings, as it allows a fast, almost real-time computation of solutions and is robust to errors.

2.4.1 The backprojection operator

First, let us understand the mechanism of backprojection and see why an additional filtering step is required.

Definition 2.5. The adjoint $\mathcal{R}^* : \mathcal{S}(Z^n) \to \mathcal{S}(\mathbb{R}^n)$ of the Radon transform characterized by

$$\langle \mathcal{R}f, g\rangle_{\mathcal{S}(Z)} = \langle f, \mathcal{R}^* g\rangle_{\mathcal{S}(\mathbb{R}^n)}$$

is defined as

$$\mathcal{R}^*(x) := \int_{S^{n-1}} g(\theta, \theta \cdot x) d\theta. \tag{2.4}$$

As $\mathcal{R}^*$ integrates a function f over all planes through point x, it is also referred to as *backprojection operator* in computerized tomography. A natural interpretation is that it "smears" back all projections' values over the corresponding plane to produce an image. We have the following important results for the backprojection operator:

Theorem 2.6 ([RK96, p. 17])**.** *Let $f(x) \in \mathcal{S}(\mathbb{R}^n)$, then*

$$\mathcal{R}^*\mathcal{R}f(x) = \left|S^{n-2}\right| \|x\|_2^{-1} * f(x), \tag{2.5}$$

where $\left|S^{n-2}\right|$ denotes the area of the unit sphere in $\mathbb{R}^n$.

The above theorem states that backprojection of data gained by Radon transformation does not recover the original function, but a blurred version of it. This circumstance is depicted in Figure 3 (top right) that shows the backprojection of the Shepp-Logan head phantom (cf. [Jai89, p. 439]), a well-known sample image in the field of computed tomography.

We want to avoid the blurring that occurs in (2.5) and thus have to improve our method. Many inversion techniques of the Radon transform are based on subsequent formula and we are going to use it as starting point for derivation of filtered backprojection.

Theorem 2.7 ([RK96, p. 20])**.** *Take $f, g \in \mathcal{S}(\mathbb{R}^n)$, then*

$$(\mathcal{R}^* g) * f = \mathcal{R}^*(g * \mathcal{R}f). \tag{2.6}$$

2.4.2 Explicit inversion formula

Before we continue with the method filtered backprojection, we are going to state an explicit version for the inversion of the Radon transform. To this end, we need to define the Riesz potential of a function f.

Definition 2.8. The *Riesz potential* $\mathcal{I}^a$ for $f(x) \in \mathcal{S}(\mathbb{R}^n)$ is defined by

$$\mathcal{I}^a f := \mathcal{F}^{-1}(\|\xi\|^{-a} \hat{f}(\xi)),\ a < n,\ a \in \mathbb{R}$$

and for $g(\theta, t) \in \mathcal{S}(Z^n)$ it is defined by

$$\mathcal{I}^a g := \mathcal{F}^{-1}(\|\tau\|^{-a} \hat{g}(\theta, \tau)),\ a < n,\ a \in \mathbb{R}.$$

Now we are able to state a general inversion formula for the Radon transform. We recall the notation $\tilde{f}$ for $\mathcal{R}f$.

Theorem 2.9 ([RK96, p. 28])**.** *If $f \in \mathcal{S}(\mathbb{R}^n)$, $|a| < n$, $a \in \mathbb{R}$, then*

$$f = \frac{1}{2(2\pi)^{n-1}} \mathcal{I}^{-a} \mathcal{R}^* \mathcal{I}^{a-n+1} \tilde{f} \tag{2.7}$$

This result is valid for n-dimensional space and we can easily simplify it for two dimensional space.

Corollary 2.10. *Set $a = 0$ in (2.7) to get*

$$f = \frac{1}{2(2\pi)^{n-1}} \mathcal{R}^* \mathcal{I}^{-n+1} \tilde{f},$$

and obtain

$$f = \frac{1}{4\pi} \mathcal{R}^* \mathcal{F}^{-1}(\|\xi\| \hat{\tilde{f}}(\xi)) \tag{2.8}$$

from (2.10) in the two dimensional setting ($n = 2$).

2.4.3 Filtered backprojection

The method of filtered backprojection can be seen as a numerical implementation of formula (2.8). To derive the method we start from (2.6) however:

$$W_\epsilon * f = \mathcal{R}^*(w_\epsilon * \tilde{f}), \quad \tilde{f} = \mathcal{R}f, \quad W_\epsilon = \mathcal{R}^* w_\epsilon \tag{2.9}$$

Our idea is to find a sequence of sufficiently smooth functions w_ϵ so that W_ϵ approximates the dirac-δ-function as ϵ goes to zero. With such a sequence $W_\epsilon * f$ will be a good approximation to f for small ϵ.

We see that $w_\epsilon * \tilde{f}$ acts as a filter on our data $\tilde{f}$ and note that several choices for the filter w_ϵ can be found in literature. A standard choice is the so-called *Ram-Lak* or *ramp* filter that emphasizes high frequencies and filters out low frequencies.

2.4.4 Parallel beam protocol

Let us now apply our inversion formula to discrete projection data $\tilde{f}(\theta_j, t_k)$ available on an evenly spaced lattice:

$$\begin{aligned} \theta_j = (\cos\phi_j, \sin\phi_j), \quad \phi_j = j\Delta\phi, \quad \Delta\phi = \pi/p, \quad j = 0, \dots, p-1, \\ t_k = k\Delta t, \qquad \Delta t = \rho/q, \quad k = -q, \dots, q \end{aligned} \tag{2.10}$$

As derived in [NW01, p. 85], the discrete inversion formula is obtained by discretizing the convolution integral in a first step and then discretizing the backprojection integral in a second step. This leaves us with approximately

$$(W_\epsilon * f)(x) \approx \frac{2\pi}{p}\Delta t \sum_{j=0}^{p-1} \sum_{k=-q}^{q} w_\epsilon(x \cdot \theta_j - t_k)\tilde{f}(\theta_j, t_k) \tag{2.11}$$

In practice it is sufficient to compute the values of the convolution for $(w_\epsilon * \tilde{f})(\theta_j, t_k)$ and then obtain the values $(w_\epsilon * \tilde{f})(x \cdot \theta_j - t_k)$ that are necessary in (2.11) by interpolation.

Unless stated otherwise, backprojection images in this thesis have been computed using the Ram-Lak filter with linear interpolation, as can be done with the following MATLAB® command:

```
iradon(R,theta,'linear','Ram-Lak');
```

We will now concentrate on the tomographic problem in two dimensions, where we will identify unit vector θ with an angle ϕ, as we have done before. This is our preferred way of parametrization in two dimensions and wherever we write $R(\phi, t)$, it has the same meaning as $R(\theta, t)$ with $\theta = (\cos\phi, \sin\phi)$.

2.5 Sinogram representation of projection data

A visual representation of the raw data retrieved by one tomography scan is called *sinogram*. It can be seen as a two-dimensional image of the attenuation coefficient and is created by plotting the Radon transform $\mathcal{R}f$ to as grayscale image.

We already noticed that the Radon transform is an even function $\mathcal{R}f(\phi, t) = \mathcal{R}f(\phi + \pi, -t)$ and thus it is sufficient to consider data only in a connected angular range $[\phi_0, \phi_0 + \pi]$, $\phi_0 \in [0, \pi]$, as data in the remaining range can be obtained through easy computation. We call data of this form *full tomographic data*.

In our sinogram representation the x-axis corresponds to the angle of the ray and subsequently the y-axis corresponds to the distance of the ray from the center (projection displacement). Figure 3 (bottom left) displays a sinogram representation of the Shepp-Logan head phantom.

2.6 The limited angle tomography problem

Main subject of this thesis is the reconstruction problem of limited angle tomography. This problem arises naturally in applications like digital breast tomosynthesis, dental tomography or electron microscopy, where a limitation of the angular range is necessary due to various reasons (e.g. X-ray dose decrease, time constraints when imaging moving objects, or X-rays being obstructed when passing through high-density regions). In such a situation we are presented with highly incomplete data, which leads to a severely ill-posed problem. The traditional reconstruction methods are not suited for this situation and produce low quality output (cf. [Fri13]).

To state our limited angle situation more precisely, let us consider a problem, where data is missing for an angular double cone $\mathcal{C}_{\phi_1,\phi_2}$, defined by $\mathcal{C}_{\phi_1,\phi_2} := ([\phi_1, \phi_2] \cup [\phi_1 + \pi, \phi_2 + \pi])$, $\phi_1, \phi_2 \in [0, \pi]$, as *limited angle tomography problem*.

As a consequence of the incomplete data, image artifacts appear in reconstructed images cf. Figure 3 (middle right). These artifacts are located on straight lines and extend over the whole reconstruction area, whereby they appear to emerge from smudging of actually existing singularities.

Goal of this bachelor's thesis was to find a method that reduces the artifacts inherent to the limited angle problem by manipulating underlying sinogram data in a suitable way. In the following chapters, we present and evaluate two methods that we have come up during research.

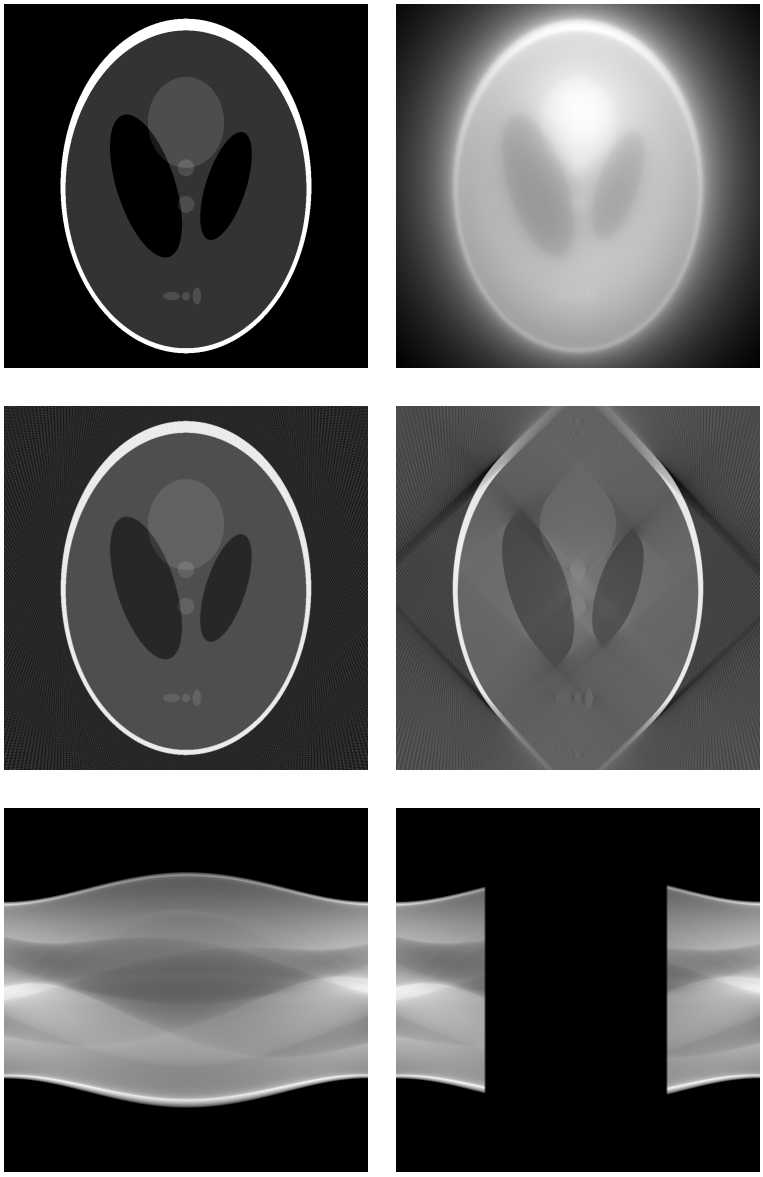

Figure 3 – The well-known Shepp Logan phantom (top left) with various of its reconstructions: unfiltered backprojection (top right), filtered backprojection of complete data (middle left) and filtered backprojection of limited angle data (middle right). Underlying projection data is displayed in the bottom row. Data in the limited angle case is only available within the range $\phi = [-\pi/4, \pi/4]$.

3 Range consistent sinogram restoration for ellipses

During this chapter we are going to take a reconstruction approach that recovers projection data for the full angular range and see that resulting sinograms satisfy some of the Ludwig-Helgason consistency conditions. Fulfillment of these conditions is a necessary prerequisite for projection data to lie in the range of the Radon transform.

We consider the discrete limited angle tomography problem in two dimensions, where angles in the angular double cone $\mathcal{C}_{\phi_1,\phi_2}$ are missing. Furthermore we assume that we are given projection data $\mathcal{R}f$ for a sufficient number of angles and projections, so that reconstruction artifacts arise solely from the limited angle situation and not from angular undersampling. Our goal is to derive an algorithm that recovers a full angle sinogram for images fitting our model, based on the strong assumption that images being examined are a superposition of various ellipses. On one hand this problem is obviously oversimplified, on the other hand it already captures well essential features of the more general problem. We hope to gain insight on the problem and intend to use some of the results obtained for a further approach regarding a more general model.

To begin with, we derive a method that works for the image of a single ellipse. We show that it is possible to transform known projections to match a fitted curve of singularities. We then extend the technique to images of multiple ellipses, that provide projections where the support of each ellipse is separate. This situation allows an easy enhancement of our procedure for these images. Thereafter we outline the procedure to enhance our method for general images of overlapping ellipses theoretically, noticing that several practical obstacles have to be overcome.

3.1 Sinogram restoration for a single ellipse

When studying the consequences of a limited angular range to the reconstruction problem for an image of ellipses, it became evident that the position of singularities in the Radon domain is characterizing their sinogram up to a factor necessary for determining the correct grey-level. Over the course of this section, we want to deduce how we can transform the projection of an ellipse at an angle ϕ_2 to the projection at an angle ϕ_1, if we only know the position of its singularities in the Radon domain for these angles.

Throughout this chapter we identify the singularities of a function with its jump points. This definition is quite informal and we will give a more mathematical definition in 4.5.

3.1.1 Analytical formula for projections of an ellipse

Beginning with the indicator function of an ellipse $\frac{x^2}{a^2} + \frac{y^2}{b^2} \leq 1$, we obtain a more general characteristic function by rotating the coordinate system counter-clockwise and subsequently translating its center to (x_0, y_0).

For the description of an ellipse it is sufficient to know its axes a and b, its rotation angle α, and the translation coordinate (x_0, y_0). We store these values in a parameter vector p.

Definition 3.1. Given parameter vector $p = (a, b, x_0, y_0, \alpha)$ with $a, b \in \mathbb{R}^+$, $x_0, y_0 \in \mathbb{R}$ and $\alpha \in [0, 2\pi]$ we define the *characteristic function of an ellipse* $\mathbb{E}_p(x, y)$ as

$$\mathbb{E}_p(x,y) := \begin{cases} 1 & \text{for } \dfrac{((x-x_0)\cos\alpha + (y-y_0)\sin\alpha)^2}{a^2} + \dfrac{((-x-x_0)\sin\alpha + (y-y_0)\cos\alpha)^2}{b^2} \leq 1 \\ 0 & \text{otherwise.} \end{cases}$$

and its projections $\mathbb{P}_p(\phi, t)$ as

$$\mathbb{P}_p(\phi,t) := \int_{L(\theta,t)} \mathbb{E}_p(x,y)dx$$

whereby $\theta = (\cos\phi, \sin\phi)$, $\phi \in [0, 2\pi]$ and $t \in \mathbb{R}$.

Ellipses have been used as prototypes in the field of computed tomography for a long time and analytical formulas for its projections are well known. We start out from the formula found in [CM01, p. 56] and apply the same coordinate transformations, as we have done for derivation of the indicator function. By doing so, we obtain an analytical formula for the projections of our general ellipse.

Proposition 3.2. *Given an ellipse $\mathbb{E}_p(x, y)$ parameterized by $p = (a, b, x_0, y_0, \alpha)$ we have the following statement regarding its projections $\mathbb{P}_p(\phi, t)$*

$$\mathbb{P}_p(\phi,t) = \frac{c}{a_\alpha^2(\phi)}\sqrt{a_\alpha^2(\phi) - (t - s\cos(\gamma-\phi))^2}, \tag{3.1}$$

whereby

$$c := 2AB, \qquad a_\alpha^2(\phi) := a^2\cos^2(\phi-\alpha) + b^2\sin^2(\phi-\alpha),$$
$$s := \sqrt{x_1^2 + x_2^2}, \qquad \gamma := \arctan(x_2/x_1),$$

whenever the term under the root is not negative and zero otherwise.

One can readily recognize that for each projection two singularities exist, each at the point where the expression inside of the square root is equal to zero.

3.1.2 Re-computation of an ellipses' projection at one angle for another angle

In the following we want to derive, how we can compute the projection of an ellipse at an arbitrary angle ϕ_2, when we are given the ellipses' projection at an angle ϕ_1 and the location of its singularities for both angles. The following proposition reveals how one projection can be transformed into any other projection. We will subsequently see that required projection parameters can be obtained from position of singularities.

Proposition 3.3. *Given $\phi_1, \phi_2 \in [0, 2\pi]$, we get*

$$u\mathbb{P}_p(\phi_1, ut + w) = \mathbb{P}_p(\phi_2, t), \tag{3.2}$$

whereby u, w are understood as

$$u := \frac{a_\alpha(\phi_1)}{a_\alpha(\phi_2)},\ w := s\cos(\gamma-\phi_1) - us\cos(\gamma-\phi_2).$$

Proof.

$$\begin{aligned}
\mathbb{P}_p(\phi_2, t) &= \frac{c}{a_\alpha^2(\phi_2)} \left(a_\alpha^2(\phi_2) - \big(t - s\cos\left(\gamma - \phi_2\right)\big)^2 \right)^{\frac{1}{2}} \\
&= \frac{c}{a_\alpha^2(\phi_1)} \underbrace{\frac{a_\alpha^2(\phi_1)}{a_\alpha^2(\phi_2)} \left(\frac{a_\alpha^2(\phi_2)}{a_\alpha^2(\phi_1)} \right)^{\frac{1}{2}}}_{u} \left(a_\alpha^2\left(\phi_1\right) - \underbrace{\frac{a_\alpha^2\left(\phi_1\right)}{a_\alpha^2\left(\phi_2\right)}}_{u^2} \big(t - s\cos\left(\gamma - \phi_2\right)\big)^2 \right)^{\frac{1}{2}} \\
&= u \frac{c}{a_\alpha^2(\phi_1)} \left(a_\alpha^2(\phi_1) - \big(ut - us\cos(\gamma - \phi_2)\big)^2 \right)^{\frac{1}{2}} \\
&= u \frac{c}{a_\alpha^2(\phi_1)} \left(a_\alpha^2(\phi_1) - \big(ut + w - s\cos(\gamma - \phi_1)\big)^2 \right)^{\frac{1}{2}} \\
&= u\mathbb{P}_p(\phi_1, ut + w)
\end{aligned}$$

□

The following lemma states that transformation parameter $a_\alpha(\phi)$ is half the width of an ellipses' projection and therefore it can be computed from its singularities in the Radon domain.

Lemma 3.4. *Assume $\mathbb{P}_p(\phi, t)$ is singular at t_1 and t_2. It holds*

$$a_\alpha(\phi) = \frac{|t_1 - t_2|}{2}. \tag{3.3}$$

Proof.

$$\begin{aligned}
\mathbb{P}_p(\phi, t) \text{ is singular at } t_{1/2} \;&\Leftrightarrow\; a_\alpha^2(\phi) - (t_{1/2} - s\cos(\gamma - \phi))^2 = 0 \\
&\Leftrightarrow\; a_\alpha(\phi) = \pm(t_{1/2} - s\cos(\gamma - \phi)) \;\Leftrightarrow\; 2a_\alpha(\phi) = |t_1 - t_2|
\end{aligned}$$

□

The translation parameter w can be obtained from a pair of points in the target and source projection, as it is independent of t and thus constant for fixed angles ϕ_1, ϕ_2. We summarize our results in the following statement of this subsection.

Proposition 3.5. *Given the singularities of an ellipses' projections at two distinct angles ϕ_1 and ϕ_2, we can compute the transformation parameters u and w of formula* (3.2)*. Thus we can transform one projection into the other (cf. Proposition 3.3).*

Proof. Obtain u by applying Lemma 3.4 to $u = a_\alpha(\phi_1)/a_\alpha(\phi_2)$. Then observe that we get w by computing the translation related to a pair of singularities, and by using the property that w is constant for fixed ϕ_1, ϕ_2. □

3.1.3 Estimating position of singularities in the sinogram of an ellipse

The next challenge is to approximate singularities for unknown projections. This is a two fold task; one first has to determine the position of singularities in the range of available data, following which one has to estimate the location of singularities in the range of unknown data.

In the case of a single ellipse it is an easy task to determine its singularities. As we have already seen, each projection has two of them, at the locations where it transitions from zero to positive or vice versa. The situation is more complicated in the case of multiple ellipses, as their projections generally overlap at some point.

Since it is a difficult subject on its own, detection of singularities is not part of this thesis. The approach made in [Rag04] incorporates both local and global data, which seems a suitable way to reliably detect singularities in given sinograms. We are primarily interested in gaining insight to the reconstruction problem and choose not to deal with the details of implementation. Therefore we choose to pick singularities manually.

Now that we know the location for each curve of singularities in the range of available data, we can obtain the approximate position of missing singularities by fitting a polynom to each curve in least squares sense. If we approximate with a polynom of sufficiently high degree, this is a natural fit, as the curves are adequately well-behaved.

3.1.4 Implementation of the approach

Let us summarize the results regarding the restoration problem of a single ellipses' sinogram: We detect curves of singularities in the range of available data, expand them over the range of missing data by least-squares fitting a polynom of sufficiently large degree and thereafter use transformation formula (3.2) to calculate missing projections from a known projection. By doing so we obtain approximated sinogram data.

This approach is detailed in algorithm 1a below and a listing of its MATLAB® implementation can be reviewed in appendix A.

Algorithm 1a.

1. *Determine position of singularities in range* $[0, 2\pi] \setminus \mathcal{C}_{\phi_1,\phi_2}$ *by looking for the position where each projection transitions from zero to non-zero or vice versa.*
2. *Use singularities obtained in Step 1 to calculate coefficients of a least-squares polynomial fit for both curves of singularities.*
3. *Generate projection data for each unknown angle* $\phi_m \in \mathcal{C}_{\phi_1,\phi_2}$ *from a known projection* ϕ_a*:*
   a) *Estimate singularities at angle* ϕ_m *by evaluating polynomials gained in Step 2.*
   b) *Calculate parameter* u *(cf. 3.2) by dividing the distance of singularities at known angle* ϕ_a *through the distance of singularities at the unknown angle* ϕ_m*.*
   c) *Calculate* w *as the signed distance of the smaller (with respect to* t*) singularity at* ϕ_a *from the corresponding singularity at the unknown angle* ϕ_m*.*
   d) *Obtain projection* $\mathbb{P}_p(\phi_m, t_k)$ *trough linear interpolation of the projection at* ϕ_a *alongside the formula* $\mathbb{P}_p(\phi_a, ut_k + w)$*. Hereby* t_k *is the discrete projection displacement from our parallel beam protocol* (2.10)*.*

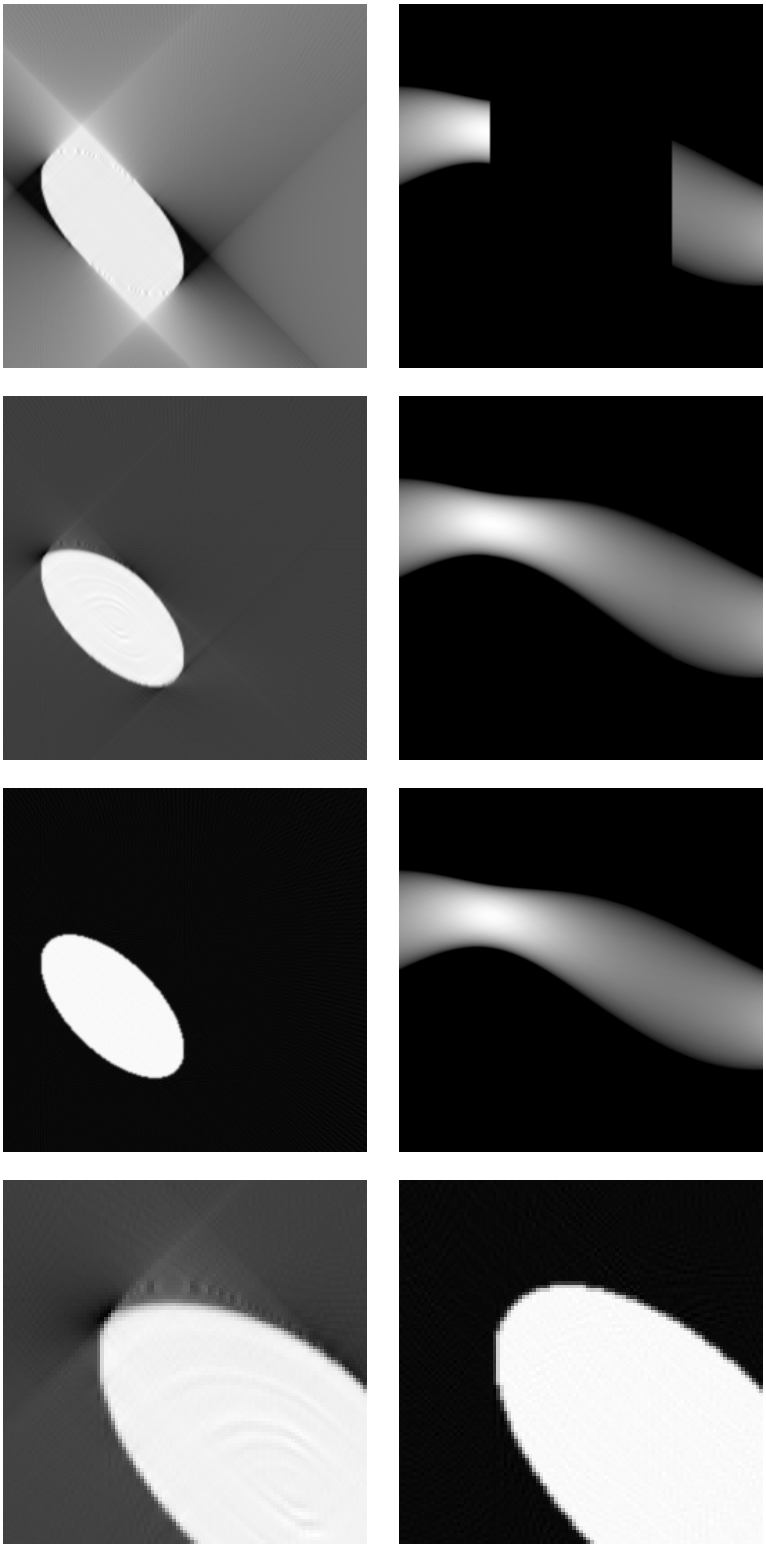

Figure 4 – Various backprojections of a single ellipse alongside with their corresponding sinograms are depicted in the first to third row; first row: reconstruction from limited angle data (PSNR 13.75 dB), second row: reconstruction from data obtained by Algorithm 1a (PSNR 25.11 dB), third row: reconstruction from full angle tomographic data (PSNR 32.45 dB). A zoomed-in view on the reconstructions gained from the restored and the full angle sinogram is given in the last row.

Outcome of this algorithm for a sample ellipse and a comparison with reconstruction from limited angle data, as well as full tomographic data is displayed in Figure 4.

Before we expand our algorithm to multiple ellipses, let us point out why we do not attenuate recovered projections.

3.2 Ludwig-Helgason consistency conditions

It is obvious that we will make a certain error in the recovery process of a projection. In order to compensate for this error it seems reasonable to attenuate the projection. As this will result in a violation of the consistency conditions however, and as our strong model assumptions keep the error fairly small, we chose not to attenuate the projections in our first approach.

Let us now see, which conditions have to be fulfilled for range consistency. Range of the Radon transform is not arbitrary, but rather characterized by the so-called *Ludwig-Helgason consistency conditions* that are also referred to as *moment conditions* in literature. We recapitulate their statement for a two dimensional setting in the following theorem.

Theorem 3.6 ([WP90, Theorem 1])**.** *It is a necessary and sufficient requirement for a given function $\tilde{f}(\theta, t)$ to be the Radon transform of a function $\tilde{f}(\theta, t)$, to satisfy the following conditions:*

1. *$\tilde{f} \in \mathcal{S}(Z^2)$ and even, i.e. $\tilde{f}(\theta, t) = \tilde{f}(-\theta, -t)$.*

2. *The integral*

$$\int_{-\infty}^{\infty} \tilde{f}(\theta, t) t^k dt \tag{3.4}$$

is a homogeneous trigonometric polynomial of degree k in θ for each $k \in \mathbb{Z}^+$.

From here we can acquire an important geometric condition for the Radon transform known as *constant body mass*.

Corollary 3.7 ([WP90])**.** *Set $k = 0$ to receive the first order consistency condition*

$$\mu = \int_{-\infty}^{\infty} \tilde{f}(\theta, t) dt = \int_{\mathbb{R}^2} f(x) dx \quad \forall \theta \in S^1. \tag{3.5}$$

One notices easily that attenuation of projections would result in violation of this geometric condition. On the other hand integration by substitution reveals that a sinogram recovered by Algorithm 1a satisfies it:

$$\int_{-\infty}^{\infty} \tilde{f}(\theta, ut + w) \cdot u \, dt = \int_{-\infty}^{\infty} \tilde{f}(\theta, u') \, du'.$$

3.3 Extension of the method to further, more complex objects

We now want to find a solution for the case of an image f that is built up from a sum of ellipses, i.e. $f = \sum_i c_i \mathbb{E}_{p_i}$. Due to linearity of the Radon transform we are able to represent the sinogram of such an image as the sum of its ellipses' projections: $\mathcal{R}f = \sum_i c_i \mathbb{P}_{p_i}$.

This situation presents us with another obstacle. For each ellipse we need a reference projection that we can transform alongside our formula (2.10). In the case where we have at least one projection with separate regions of each ellipses' support, we can simply divide this projection as we will do in the next subsection. If projections of two or more ellipses overlap for each angle however, we have to determine which values belong to each ellipse. We will outline how this task can be solved in the next subsection but one.

3.3.1 Multiple ellipses that can be separated in a projection

In the case of multiple ellipses we restrain to a manual inspection for the task of determining singularities of each ellipse. To do so, a polynom is fitted to hand-picked reference points in the sinogram. Our approach is represented in Figure 5.

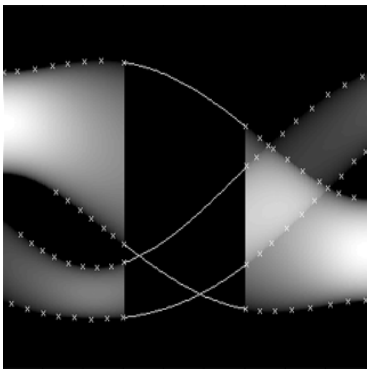

Figure 5 – A polynom is fitted to hand picked reference points for each curve of singularities.

As previously indicated we now suppose to have at least one angle ϕ_a for which the projections $\mathbb{P}_{p_i}(\phi_a, t)$ have distinct support. Hereby the support of each projection is given by the region between its singularities respectively. We can now divide $\mathcal{R}(\phi_a, t)$ into the particular $\mathbb{P}_{p_i}(\phi_a, t)$ by setting values lying outside the support of the respective projection to zero.

After doing so, we possess location of singularities and a reference projection for each ellipse. Thus we can continue the same way, as we did for a single ellipse. We summarize our approach in Algorithm 1b below. A listing of its MATLAB® implementation can be reviewed in appendix A.

Algorithm 1b.

1. *Determine the position of singularities in range* $[0, 2\pi] \setminus \mathcal{C}_{\phi_1,\phi_2}$ *by manual inspection and extend these singularities over range* $\mathcal{C}_{\phi_1,\phi_2}$ *through a least-squares polynomial fit.*
2. *For each pair of singularities procede with Steps 3a to 3d of Algorithm 1a. Obtain the necessary reference projection from* $\mathcal{R}(\phi_a, t)$ *by setting values lying outside the support of respective projection to zero. The reconstructed sinogram is a sum of the sinograms for each ellipse respectively.*

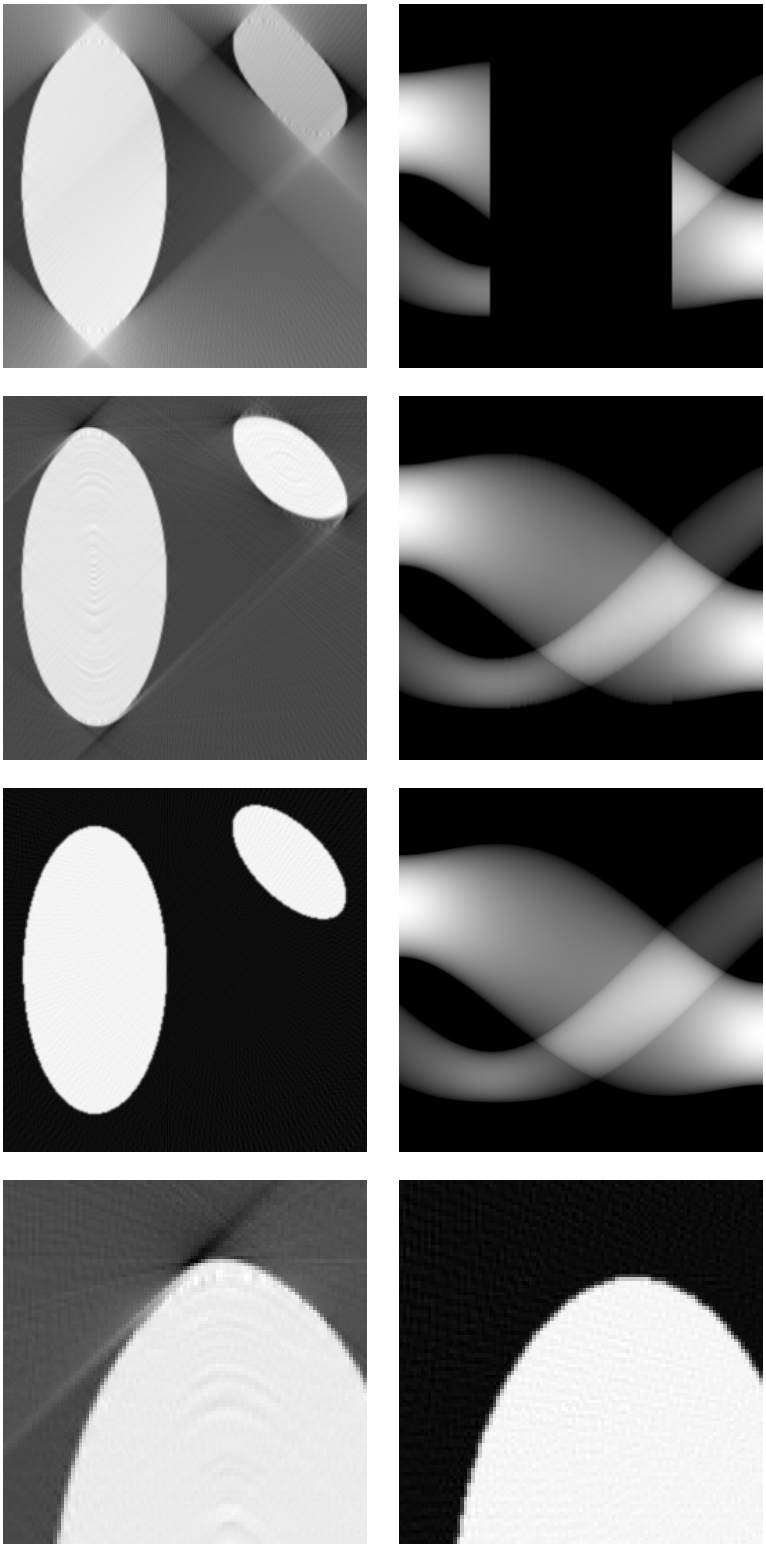

Figure 6 – Various backprojections of two ellipses alongside with their corresponding sinograms are depicted in the first to third row; first row: reconstruction from limited angle data (PSNR 11.13 dB), second row: reconstruction from data obtained by Algorithm 1a (PSNR 21.08 dB), third row: reconstruction from full angle tomographic data (PSNR 28.76 dB). A zoomed-in view on the reconstructions gained from the restored and the full angle sinogram is given in the last row.

Outcome of this algorithm for a sample image of two ellipses and a comparison with reconstructions from limited angle data and full tomographic data is displayed in Figure 6.

3.3.2 General idea for all images solely made up from ellipses

Let us now outline the procedure for the case, when the projection data for some ellipses overlaps in a way that we cannot split the sinogram data into separate parts for each ellipse respectively.

We are given a sinogram of the form $\mathcal{R}f = \sum_i c_i \mathbb{P}_{p_i}$. As we already know the singularities for each ellipse, we can calculate $\mathbb{P}_{p_i}(\phi_a, t_k)$. Hereby t_k denotes the discrete projection displacement from our parallel beam protocol (2.10).
Now we know the amount each ellipse contributes to a specific point in the sinogram up to its coefficient c_i. We obtain this coefficient by solving an overdetermined system of linear equations in the least-squares sense.

$$\begin{pmatrix} \mathbb{P}_{p_1}(\phi_a, t_k) & \dots & \mathbb{P}_{p_n}(\phi_a, t_k) \end{pmatrix} \begin{pmatrix} c_1 \\ \vdots \\ c_n \end{pmatrix} = \begin{pmatrix} \mathcal{R}f(\phi_a, t_k) \end{pmatrix}$$

As we can already evaluate the quality of our approach from Algorithm 1b, we will not conduct a practical implementation of this generalization here.

3.4 Conclusion of the method

Over the course of this chapter we have proposed an approach to recover an image from limited angle tomographic data. Thereby we have employed a model that assumes the image we want to recover is comprised of various ellipses. Under this strong assumption, we could derive a method that is able to compute full angle tomographic data from limited angle sinograms.

Reconstructions of obtained full angle data has approximated the shape of ellipses somewhat better than reconstructions from the initial limited angle sinograms. Our approach has significant drawbacks however. At first it is to mention that the practical relevance of ellipse reconstruction is very limited for real-world applications. One could argue that it is possible to apply our method to images that do not meet the model conditions. This strategy results in guessing of a significant amount of information however, and we are not guaranteed that resulting reconstructions do not contain considerable misinterpretations of the situation, as we have evaluated in concise experiments. In the second place it remains to say that artifacts originating from the limited angle situation are not completely removed and closer inspection of reconstructions reveals that even additional circular artifacts are created by our procedure.

4 Smooth truncation of sinogram data through local extension near cut-off edges

Over the course of this chapter we consider the same limited angle tomography problem as we did in the previous chapter, i.e. projections are missing for the angular double cone $\mathcal{C}_{\phi_1,\phi_2}$. Since we have seen that a range consistent full angle reconstruction has significant shortcomings, we will extend available projections only within a local neighbourhood this time.

In the following it is our goal to develop an algorithm that does not impose additional conditions on the original image. We want to find a method that avoids to add a significant amount of additional information to the sinogram and incorporates as much of the information available in projections as possible.

We will interpret our findings in the context of microlocal analysis that we introduce in the following.

4.1 Micro-local analysis

Main purpose of this section is to familiarize the reader with the framework of microlocal analysis. Important results concerning the Radon transform will be summarized and some expectations for a reconstruction algorithm that we subsequently develop are presented.

The general idea behind microlocal analysis is to investigate a function not only by localizing in space through the use of cut-off functions, but also by microlocalizing with respect to the cotangent space of directions at a given point through methods based on Fourier transforms.

At first we are going to introduce an important microlocal concept, the wavefront set of a distribution, which was coined by Lars Hörmander in [Hör71]. Following that we will familiarize ourselves with statements on the wavefront set of the Radon transform and their impact on limited angle tomography, as developed by Eric T. Quinto in [Qui93].

4.1.1 Mathematical prerequisites

Let us now recall some mathematical concepts that we will need during the rest of this chapter. We begin with definition of distributions, which can be seen as objects that generalize functions.

Definition 4.1. A *distribution* is a continuous linear functional that maps the space of compactly supported test functions $\mathcal{D}(\mathbb{R}^n) := \{f \in C^\infty(\mathbb{R}^n) : f \text{ has compact support}\}$ to the set of real numbers. We want to denote distributions by $\mathcal{D}'(\mathbb{R}^n)$.

We say a distribution f has compact support, if there is a compact set $K \subseteq \mathbb{R}^n$, such that $f(\phi) = 0$ for all functions $\phi \in \mathcal{D}(\mathbb{R}^n)$ with support disjoint from K and denote the set of distributions with compact support as $\mathcal{E}'$.

The concept of singularities, that we have used in previous sections without a clear definition, shall be brought to a more mathematical standing with the following definition.

Definition 4.2 ([Hör71, p. 120])**.** Define the *singular support* of a distribution $f \in \mathcal{D}'(\mathbb{R}^n)$ as

$$\operatorname{sing\,supp} f := \bigcap_{\substack{\phi \in C^\infty(\mathbb{R}^n), \\ \phi f \in C^\infty(\mathbb{R}^n)}} \{x \in \mathbb{R}^n : \phi(x) = 0\}. \tag{4.1}$$

We can interpret the singular support of a distribution f as the set of all points, where it is not smooth (its discontinuities). Here we have localized f by multiplying it with a cut-off function ϕ.

Before we can introduce the wavefront set WF, we still need two definitions. Namely the conical neighborhood of a set in $\mathbb{R}^n$:

Definition 4.3. A neighborhood N of $X \subseteq \mathbb{R}^n$ is called *conic*, if

$$t\xi \in N \quad \forall \xi \in N,\ t > 0.$$

and the definition of a rapidly decaying distribution:

Definition 4.4. We say a distribution $f \in \mathcal{D}'(\mathbb{R}^n)$ is *rapidly decreasing* in $X \in \mathbb{R}^n$, if it decays faster than any negative power of its variable x. That is, for every number N there exists a constant C_N so that

$$|f(x)| \leq C_N(1 + |x|)^{-N} \quad \forall x \in X.$$

Now we are ready to introduce the main object of our inspection in this chapter, the wavefront set of a distribution.

4.1.2 Wavefront set of a distribution

The wavefront set characterizes the singularities of a distribution in space and with respect to its Fourier transform at each point. It was originally coined by Lars Hrmander, but we want to use a definition of Quinto as it is more suited for the analysis of our limited angle problem.

Definition 4.5 ([Qui93, Definition 2.1])**.** Let $f \in \mathcal{D}'(\mathbb{R}^n)$, $x \in \mathbb{R}^n$ and $\xi \in \mathbb{R}^n \setminus 0$. Then we say $(x, \xi) \in WFf$, the *wavefront set* of f, if and only if for each cut-off function $\phi \in \mathcal{D}(\mathbb{R}^n)$ at x with $\phi(x) \neq 0, \mathcal{F}(\phi f)$ does not decrease rapidly in any open conic neighbourhood of the half ray $\{t\xi : t > 0\}$.

In more familiar terms, WF(f) tells not only where the function f is singular (which is already described by its singular support), but also in which direction the singularity occurs. The singular support of a distribution f can be obtained from the wavefront set WF(f) by projecting it to its first coordinate.

4.1.3 Correspondence of singularities in f and $\mathcal{R}f$

Application of the microlocal method to limited angle tomography, as first described by Eric T. Quinto, provides insight on singularities in reconstructed images. The following theorem establishes a connection between singularities in f and $\mathcal{R}f$. Based upon that we can determine which singularities we can faithfully reconstruct and which additional singularities we have to expect from limited angle data.

Theorem 4.6 ([Qui93, Theorem 3.1])**.** *Assume* $f \in \mathcal{E}'(\mathbb{R}^2),\ x \in L(\theta, t),\ (\theta, t) \in Z^2,\ a \neq 0$ *and* $\zeta := (-x \cdot \theta^{\perp}, 1)^{\top}$*, then:*

$$(x, a\theta) \in \mathrm{WF}\, f \quad \Leftrightarrow \quad ((\theta, t), a\zeta) \in \mathrm{WF}\, \mathcal{R}f. \tag{4.2}$$

The theorem bears a powerful statement, as it implies an *exact* correspondence between the wavefront set of a function f and the wavefront set of its Radon transform $\mathcal{R}f$.

As already mentioned, we can use this result to determine which singularities we can faithfully identify from limited angle data. Other singularities appear smoothed in reconstructed images.

Corollary 4.7 ([Qui93, Corollary])**.** *Only singularities where the direction is available in limited angle data, can be reconstructed in a stable way. We call*

$$\mathrm{WF}_{\phi_1,\phi_2} := \{(x, \theta) : (x, \theta) \in \mathrm{WF}(f),\ \theta = (\cos\phi, \sin\phi),\ \phi \in [0, 2\pi] \setminus \mathcal{C}_{\phi_1,\phi_2}\}$$

the set of visible singularities *of* f*.*

Inspired by the representation in [Fri12, p. 42], we have depicted the set of visible singularities for a centered circle and for the Shepp-Logan phantom by red lines in Figure 7. The limited angle reconstructions of these images clearly show that visible singularities are faithfully reconstructed and other singularities, in contrary, are not distinguishable or smoothed out.

The reconstructions in Figure 7 also expose another phenomenon. We are not only missing some singularities of underlying function f, but we are further confronted with additional singularities. These additional singularities seem to originate from existing singularities at the edge of cut-off angles and are streaked over the entire reconstruction image in straight lines. We find the following useful proposition.

Proposition 4.8 (cf. [Fri12, Theorem 3.24])**.** *Consider a function* $f \in \mathcal{E}'(\mathbb{R}^2)$*. Then the wavefront set of a reconstruction from limited angle data with cut-off angles* ϕ_1, ϕ_2 *is contained in*

$$\mathrm{WF}_{\phi_1,\phi_2}(f) \cup\ \mathcal{A}_{\phi_1,\phi_2}(f)$$

where $\mathrm{WF}_{\phi_1,\phi_2}(f)$ *is the set of visible singularities from proposition 4.7 and*

$$\mathcal{A}_{\phi_1,\phi_2}(f) := \Big\{(x + r\theta^{\perp}, a\theta) : (x, \theta) \in \mathrm{WF}(f),\ a, r \neq 0,\ \theta = (\cos\phi, \sin\phi),\ \phi \in \{\phi_1, \phi_2\}\Big\}$$

is the set of additional singularities*.*

This proposition reveals that the wavefront set of reconstructed images can contain additional singularities besides to the recovered visible singularities. These additional singularities originate from singularities with direction along the cut-off angles ϕ_1 and ϕ_2.

In the following subsection we will apply this knowledge to our limited angle problem.

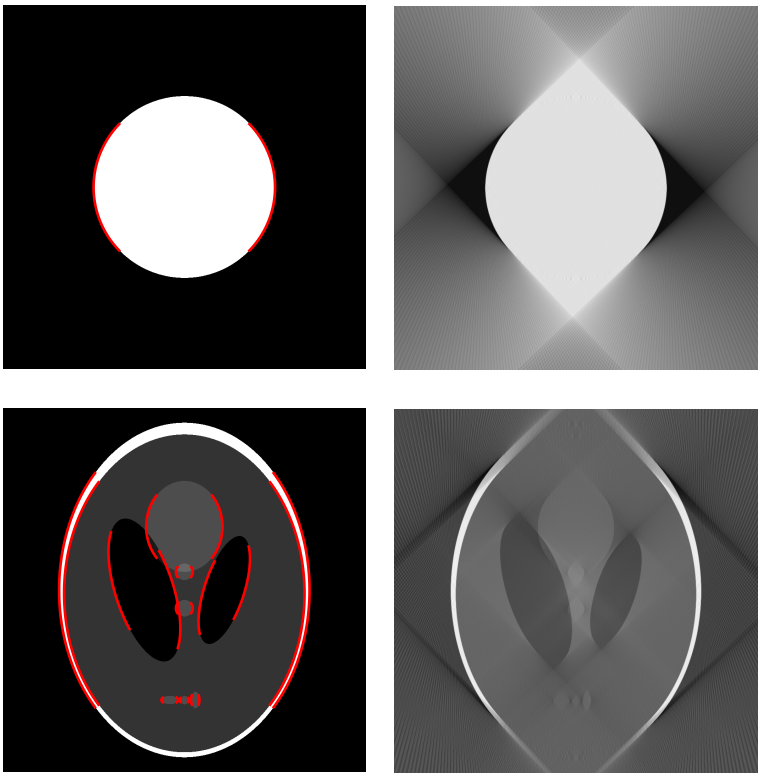

Figure 7 – Analysis of reconstructions from limited angle data with cut-off angles $\phi_1 = 46°, \phi_2 = 135°$. The objects investigated are a simple disc and the Shepp-Logan phantom. Inspired by the representation in [Fri12, p. 42], we indicate visible singularities with red lines (left). Additional artefact singularities are streaked over the entire reconstruction along lines perpendicular to the cut-off angles (right).

4.2 Idea for a microlocal approach

Goal of this subsection is to derive a method which manipulates given limited angle data such that artifact singularities are reduced, while keeping as much information contained in the sinogram as possible.

We can explain missing singularities (these are singularities, for which the angle of direction is not available in limited data) simply through lack of information. On the other side of the spectrum, artifact singularities can be explained by singularities that are introduced in the Radon domain trough abrupt truncation of data at cut-off angles. These singularities have a direct counterpart in the image domain, as predicted by Quinto's theorem 4.6.

Thus, in order to avoid artifact singularities, we have to circumvent hard truncation of data. An approach made by [Fri12], is to multiply limited angle data with a smooth truncation function that leads to a gradual decrease of values to the edges of available data. In his thesis he showed that this procedure reduces limited angle artifacts.

Based on these results, we have come up with a novel approach that inhibits abrupt cut-off at angles ϕ_1 and ϕ_2, but in addition keeps available data intact. We accomplish this by re-using some of the results gained in Chapter 3 and extend available data to a locally limited range, which we subsequently multiply with a suitable smooth truncation function. Thus we obtain a gradual decrease of values from the edges of available data and reduce artifacts that stem from the singularities introduced by abrupt cut-off at these edges.

4.2.1 Local extension of data

Let us now describe our procedure for extending a given sinogram to missing angles in a limited local range. We will capture the most important features well, if we have a good estimation for singularities.

Similar to our procedure in Algorithms 1a and 1b, we first detect curves of singularities in the angular range of available data, this time with restriction to singularities close to the cut-off angles. In a next step we approximate these curves by fitting a polynomial of sufficiently high degree so that we can calculate the position of singularities in the unknown range.

Now that we know the position of singularities for each ellipse and projection, we transform the last available projection at a cut-off angle into the projections that we want to recover in its neighborhood. We do so by splitting the source projection in multiple parts separated by its singularities and then linearly transform these parts so that they match with the position of singularities in the target projection respectively. The so gained projection is than evaluated at the sampling points of our discrete grid.

Following this procedure, we recover a limited range of angles near both cut-off edges, i.e. $[\phi_1, \phi_1 + \epsilon]$ and $[\phi_2 - \epsilon, \phi_2]$. Each projection at an angle ϕ inside this range is attenuated through multiplication with a smooth truncation function $\Gamma_k(\phi) = (1 - \frac{\phi}{\epsilon})^k$.

Let us sum up our approach in the following algorithm, which we have implemented in MATLAB® as found for reference in Appendix A. Figure 8 depicts two sample sinograms as returned by the algorithm.

Algorithm 2.

1. *Estimate the location of singularities in a local range close to cut-off edges ϕ_1, ϕ_2.*

   a) *Detect singularities in $[\phi_1 - 2\epsilon, \phi_1]$ and $[\phi_2, \phi_2 + 2\epsilon]$.*

   b) *Obtain estimate for singularities in $[\phi_1, \phi_1 + \epsilon]$ and $[\phi_2 - \epsilon, \phi_2]$ by evaluating a polynomial fitted to available singularities.*

2. *Extend existing projection data at angles ϕ_1, ϕ_2 by matching their singularities' positions to the position of singularities at the target projection.*

   a) *For each angle ϕ that is contained in our parallel beam protocol and in the reconstruction range $[\phi_1, \phi_1 + \epsilon] \cup [\phi_2 - \epsilon, \phi_2]$, calculate a projection. Do so by splitting the source projection at ϕ_1 or ϕ_2 in multiple parts separated by its singularities and then linearly transform these parts so that they match with the position of singularities in the target projection respectively. Then evaluate this projection at the sampling points of our discrete grid.*

   b) *Hereby attenuate obtained projection through multiplication with the smooth transition function $\Gamma_k(\phi) = (1 - \frac{\phi}{\epsilon})^k$.*

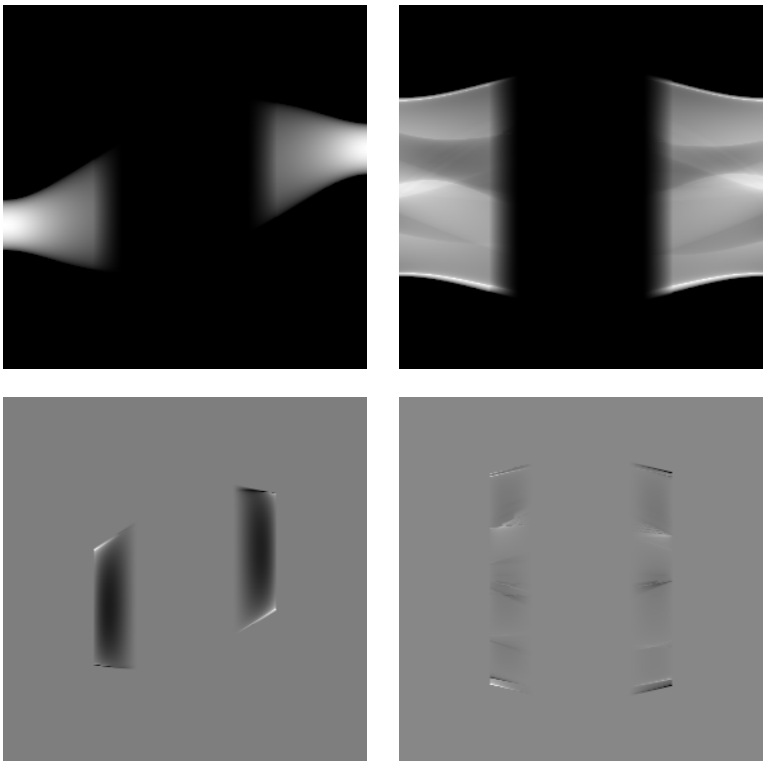

Figure 8 – Top row: sample output as returned by Algorithm 2. Bottom row: pointwise difference to output that was generated from attenuated original data. Examined objects are discussed below.

4.2.2 Advantages and disadvantages of the approach

Compared to out first approach, we immediately observe that our procedure violates the consistency conditions this time. For sensitive reconstruction methods, such as MLEM, this can lead to a non-converging situation.

As misdiagnoses can happen with the rendering of non-physical features in real-world medical applications, it is essentially necessary that only actual features of the underlying object are visible in reconstructed images

Our local approach provides a possibility to choose a trade-off between artifact reduction and information preservation in a controlled manner.

4.3 Implementation and evaluation in our case for ellipses

Concerning the practical implementation of our algorithm, we still face some technical difficulties. On one hand we have to define the behaviour for all emerging special cases, as for example when the curves of singularities overlap within our extension range. On the other hand we have to cope with flawed projections in real-world applications, as they are always corrupted by noise. Most of all, however, we still lack an efficient algorithm for detection of singularities. We also note that there are certain images, to which the approach cannot be applied without modification (e.g. smooth objects without singularities).

While all of these issues are important, we want to focus on a quick reference implementation of our algorithm. Therefore we implement the method for images constructed from overlapping ellipses. For these kind of images we know the exact curves of singularities and their derivatives from analytical formulas. This is sufficient for a first evaluation of expected outcome.

We note that this procedure is not to confuse with our first approach, where we incorporated the requirement that an image is a superposition of ellipses directly in its model. Here we only use the additional information for compensation of technical difficulties, but could apply our algorithm to other images in theory.

A short empiric study revealed that higher order Taylor approximations do not provide significant improvement over first order approximation. We further found that $k = 1.5$ is a good choice for the parameter of our smooth truncation function. Let us now have a look at some sample images.

4.3.1 Single ellipse

The outcome of Algorithm 2 for underlying image $f = c_1 \mathbb{E}_{p_1}$ is depicted in Figure 9. We see that reconstructions show less streak artifacts for increasing values of ϵ.

i	A	B	x_0	y_0	α	c_i
1	0.2	0.6	0.3	0	45	1.0

Table 1 – Ellipse parameters.

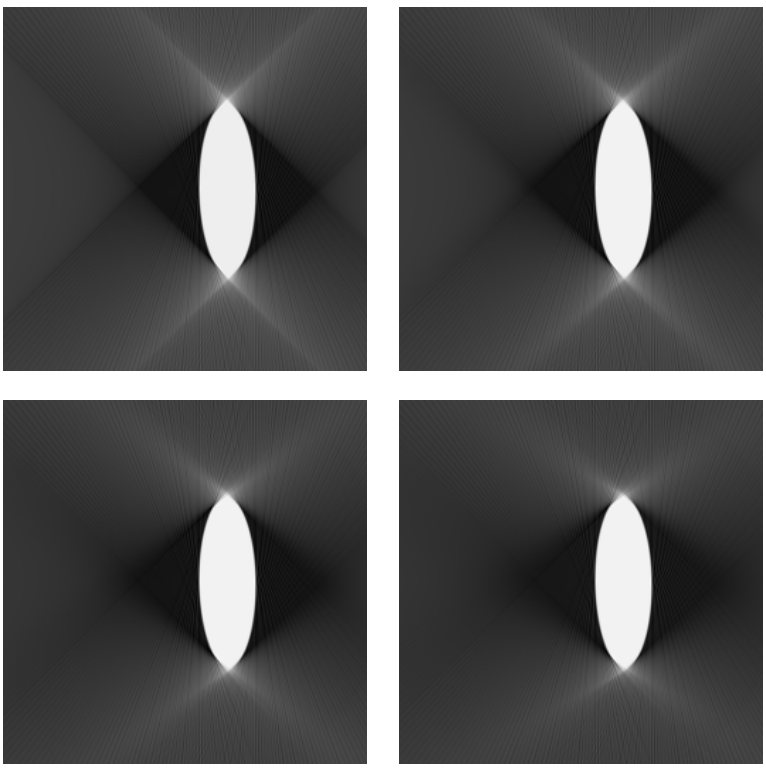

Figure 9 – Various backprojections of a single ellipse. Top-left: reconstruction from limited angle data ($\phi_1 = 46°, \phi_2 = 135°$), top-right: reconstruction employing Algorithm 2 with $\epsilon = 7°$, bottom-left: $\epsilon = 15°$, bottom-right: $\epsilon = 22°$.

4.3.2 Shepp-Logan phantom

The outcome of Algorithm 2 for underlying image $f = \sum_{n=1}^{9} c_i \mathbb{E}_{p_i}$ is depicted in Figure 10. We can see the same decrease of artifacts with increasing range of recovery, as we saw for the single ellipse. However this time we are also confronted with some additional artifacts for increasing ϵ, which can be explained by errors we introduce with our extension.

i	A	B	x_0	y_0	α	c_i
1	0.874	0.6624	0	-0.0184	90	1.0
2	0.31	0.11	0.22	0	72	-0.8
3	0.41	0.16	-0.22	0	108	-0.2
4	0.25	0.21	0	0.35	90	-0.2
5	0.046	0.046	0	0.1	0	0.1
6	0.046	0.046	0	-0.1	0	0.1
7	0.046	0.023	-0.08	-0.605	0	0.1
8	0.023	0.023	0	-0.605	0	0.1
9	0.046	0.023	0.06	-0.605	90	0.1

Table 2 – Ellipse parameters of Shepp-Logan phantom.

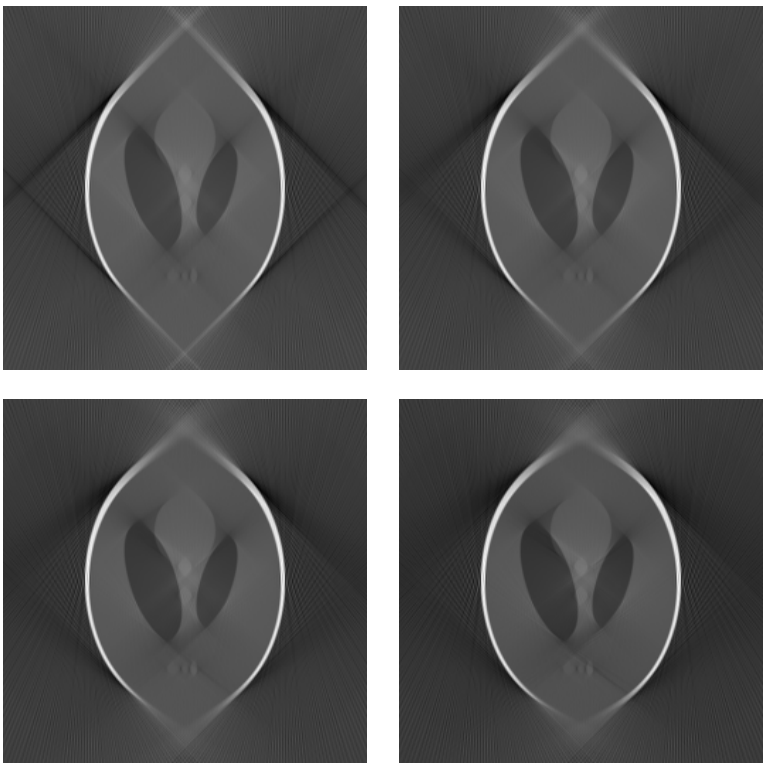

Figure 10 – Various backprojections of the Shepp-Logan phantom. Top-left: reconstruction from limited angle data ($\phi_1 = 46°, \phi_2 = 135°$), top-right: reconstruction employing Algorithm 2 with $\epsilon = 7°$, bottom-left: $\epsilon = 15°$, bottom-right: $\epsilon = 22°$.

5 Outlook and concluding remarks

Over the course of this bachelor's thesis we have learned about various aspects from the rich field of computed tomography. In an introductory chapter we have set the necessary mathematical foundations and subsequently introduced the method of filtered backprojection, as well as the problem of limited angle tomography.

This brought us to the main subject of this thesis: finding an algorithm operating on given sinogram data in order to reduce artifacts inherent to the limited angle problem. In a first approach we tried to solve this problem for objects made up solely from a superposition of ellipses. Contingent to this strong model assumption, we were able to come up with a method that allows us to recover sinogram data over the whole angular range - a requirement imposed for valid projection data by the consistency conditions. However our approach introduced additional, circular artifacts and has limited use in real-world applications.

In a next step we have re-employed the knowledge gained in our first approach together with an idea that we found in the PhD-thesis of Jürgen Frikel, to come up with a novel approach. We saw that limited angle artifacts can be avoided through smooth decay of values at the cut-off edges of available data. Novel to our approach is that we first extend sinogram data to a locally limited range in order to keep as much information, contained in sinogram data, as possible. We then multiplied this data with a smooth truncation function to obtain the desired decay into the range of missing data.

This approach turned out to be a promising way to reduce limited angle artifacts. However for a thorough implementation there are still technical difficulties to overcome. These include the detection and mapping of singularities and the handling of input that is corrupted by noise.

All in all, this bachelor's thesis has served well to become familiar with the limited angle tomography problem and proposes two methods that offer an entry point for further research. It is desirable to evaluate our microlocal approach with an automated algorithm for detection of singularities or to do further research on discretization issues.

A Matlab Code

Here we present MATLAB® implementations of suggested algorithms.

Algorithm 1a

```
1
2  %%
3  % Algorithm 1a
4  %
5  % Input:  limited angle sinogram: R_lim,
6  %           (data in the range of theta1 to theta2 is missing)
7  %         starting angle of missing data: theta1,
8  %         ending angle of missing data: theta2
9  %
10 % Output: reconstructed sinogram: R,
11 %         reconstructed image: I
12
13 function [R,I] = algorithm_1a( R, phi1, phi2, imgsize)
14
15 % Step 1: Estimate missing singularities.
16
17 % Gather location of singularities in the interval [0, theta1].
18 for x = 1:(phi1-1);
19     y_top(x) = find(R(:,x),1,'first');
20     y_bottom(x) = find(R(:,x),1,'last');
21 end
22
23 % Gather location of singularities in the interval [theta2, 179].
24 for x = (phi2+1):180
25     y_top(x-(phi2-phi1+1)) = find(R(:,x),1,'first');
26     y_bottom(x-(phi2-phi1+1)) = find(R(:,x),1,'last');
27 end
28
29 % Calculate coefficients of a polynom that fits to the existing
30 % singularities in a least squares sense.
31 x = [1:(phi1-1) (phi2+1):180];
32
33 p_top = polyfit(x,y_top,8);
34 p_bottom = polyfit(x,y_bottom,8);
35
36 % Step 2: Transform an existing projection to obtain projection data in the
37 % missing range.
38
39 for theta = phi1:phi2
40     % Calculate parameters of the transformation from fitted singularities.
41     a1 = y_bottom(phi1-1) - y_top(phi1-1);
42     a2 = polyval(p_bottom,theta) - polyval(p_top,theta);
43     u = a1/a2;
44     w = y_top(phi1-1) - u*polyval(p_top,theta);
45
46     % Actual transformation.
47     t = 1:size(R,1);
48     t = u.*t + w;
49
50     R(:,theta) = u.*interp1q((1:size(R,1))',R(:,phi1-1),t');
```

```
end

R(isnan(R))=0;

% Filtered back projection with Ram-Lak filter
I = iradon(R,0:179,'linear','Ram-Lak',1,imgsize);

end
```

Algorithm 1b

```
%%
% Algorithm 1b
%
% Input:  limited angle sinogram: R_lim,
%           (data in the range of theta1 to theta2 is missing)
%         starting angle of missing data: theta1,
%         ending angle of missing data: theta2
%
% Output: reconstructed sinogram: R,
%         reconstructed image: I
%
% Manual steps are needed for fitting of curve. From top to bottom (linke Seite).

function [R,I] = algorithm_1b(R_lim,phi1,phi2,imgsize)

% 1. Step: Manually select reference points used to interpolate polynomial
% curves for singularities.

% Plot the limited angle sinogram, where we will select reference points.
figure();imagesc(R_lim);colormap(gray)
hold on

% Number of singularity curves (should be an even number, as we each
% ellipse has exactly two curves.
num = inputdlg('Please enter the number of singularity curves:');
num = str2double(num{1});

% Degree of polynomial to be fitted.
degree = 5;

% Initialize matrix containing the coefficients of fitted polynomials.
coeff = zeros(num,degree+1);

% For each curve of singularities ...
for i = 1:num
    xy = [];
    n = 0;

    % Collect reference points by left clicking in the limited angle
    % sinogram. The last point for the current curve is selected by
    % clicking with the right mouse button.
    button = 1;
    while button == 1
        [xi,yi,button] = ginput(1);
        plot(xi,yi,'wx')
```

```
47
48          n = n+1;
49          xy(:,n) = [xi;yi];
50      end
51
52      % Fit a polynom to the singularity curve.
53      x = xy(1,:);
54      y = xy(2,:);
55
56      coeff(i,:) = polyfit(x,y,degree);
57
58      % Plot the fitted polynom in the range of missing angles.
59      xp = 0:179;
60      yp(i,:) = polyval(coeff(i,:),xp);
61
62      plot(phi1:phi2,yp(i,phi1:phi2),'w-');
63  end
64
65  hold off
66
67  % 2. Step: Obtain reference projections by dividing sinogram at one angle
68  % where supports of projections do not overlap. Without limitation we
69  % expect phi1-1 to be that angle.
70
71  for i=1:num/2
72      % Singularities for current ellipse
73      s1(i) = round(polyval(coeff(2*i-1,:),phi1-1));
74      s2(i) = round(polyval(coeff(2*i,:),phi1-1));
75
76      % Sort singularities
77      if s1(i) > s2(i)
78          temp = s2(i);
79          s2(i) = s1(i);
80          s1(i) = temp;
81      end
82
83      % Set values outside support to zero
84      p(i,:) = R_lim(:,phi1-1);
85      p(i,1:(s1(i)-1)) = zeros((s1(i)-1),1);
86      p(i,(s2(i)+1):size(R_lim,1)) = zeros(size(R_lim,1)-(s2(i)),1);
87  end
88
89  % Continue as in Algorithm 1..
90
91  R = R_lim;
92
93  % Round to integers
94  yp = round(yp);
95
96  % Transform an existing projection to obtain projection data in the missing
97  % range.
98
99  for phi=phi1:phi2
100     this_projection = zeros(size(R,1),1);
101     for i=1:num/2
102         % Calculate parameters of the transformation from fitted singularities.
103         a1 = yp(2*i,phi1-1) - yp(2*i-1,phi1-1);
104         a2 = yp(2*i,phi) - yp(2*i-1,phi);
105         u = a1/a2;
106         w = yp(2*i,phi1-1) - u*yp(2*i,phi);
```

```
107
108         % Actual transformation.
109         t = 1:size(R,1);
110         t = u.*t + w;
111
112         this_projection = this_projection + u.*interp1((1:size(R,1))',p(i,:),t');
113     end
114     R(:,phi) = this_projection;
115 end
116 R(isnan(R))=0;
117
118 I = iradon(R,0:179,'linear','Ram-Lak',1,imgsize);
```

Algorithm 2

```
1  function rec = algorithm_2( r, s, d, dd, num )
2  % r     original slice
3  % s     singularities at angle of slice
4  % d     derivative at angle of slice
5  % num   number of angles to extract
6  %
7  % rec   reconstructed part of sinogram
8
9  % Sort singularities alongside with derivatives
10 [s, IX] = sort(s);
11 d = d(IX);
12 dd = dd(IX);
13 %dd=zeros(size(dd));
14
15 rec=zeros(size(r,1),num);
16
17 for i=1:num
18 j=i * pi/180;
19 si = s + d*j + (dd/2)*(j.^2);
20 rt = resample( s, r, si )';
21
22 % Mitigation
23 mit=((num-i)/num).^1.5;
24
25 rec(:,i)=rt * mit;
26
27 end
28
29 end
30
31 function rt = resample( sing, r, singt )
32
33 % Make column vectors
34 sing=sing(:);
35 singt=singt(:);
36 r=r(:);
37
38 % Singularity vectors and image borders
39
40 s_phi=round([1;sing;size(r,1)]);
41 s_phit=[1;singt;size(r,1)];
42
```

```
43 % Calculate sampling points at target angle
44
45 nsamples=s_phi(2:end)-s_phi(1:end-1)-1;
46 spacing=(s_phit(2:end)-s_phit(1:end-1))./(nsamples+1);
47
48 sampling=[];
49 for i=1:size(nsamples,1)
50     this=(0:nsamples(i))*spacing(i)+s_phit(i);
51     sampling=[sampling this];
52 end
53 sampling=[sampling s_phit(end)];
54
55 % Re-sample to sinogram base points
56
57 resampling=1:size(r,1);
58 rt=interp1(sampling,r,resampling);
59
60 end
```

B Glossary of symbols

In the following we provide a summery of important symbols used throughout this thesis.

Symbol	Description
$C^\infty(U)$	Space of smooth functions.
$L^p(U)$	Space of p-integrable functions.
$L^p(U, d\mu)$	Space of weighted p-integrable functions.
$\mathcal{S}(\mathbb{R}^n)$	Schwartz space of all infinitely differentiable functions that rapidly decay with all their derivatives.
B_r^n	Ball with radius r in $\mathbb{R}^n$.
S^{n-1}	Unit sphere in $\mathbb{R}^n$.
$Z^n := S^{n-1} \times \mathbb{R}$	Unit cylinder in $\mathbb{R}^n$.
$L(\theta, t),$	Affine hyperplane in $\mathbb{R}^n$.
$\hat{f}(\xi) := \mathcal{F}f(\xi)$	Fourier transform.
$f(x) = \mathcal{F}^{-1}\hat{f}(x)$	Inverse Fourier transform.
$(f * g)(x)$	Convolution in $\mathbb{R}^n$.
$\tilde{f}(\theta, t) := \mathcal{R}f(\theta, t)$	Radon transformation.
$\mathcal{R}^*$	Backprojection operator.
$\mathcal{I}^a$	Riesz potential.
$\mathcal{C}_{\phi_1,\phi_2}$	Angular double cone.
$\mathbb{E}_p(x, y)$	Characteristic function of an ellipse with parameter vector p.
$\mathbb{P}_p(\phi, t)$	Projection of ellipse with parameter vector p.
$\mathrm{WF}(f)$	Wavefront set.
$\mathrm{WF}_{\phi_1,\phi_2}(f)$	Set of visible singularities.
$\mathcal{A}_{\phi_1,\phi_2}(f)$	Set of additional singularities.

Bibliography

[CM01] Kak Avinash C. and Slaney Malcolm. *Principles of Computerized Tomographic Imaging*. Society for Industrial and Applied Mathematics, 2001.

[Eps08] Charles L. Epstein. *Introduction to the Mathematics of Medical Imaging*. Society for Industrial and Applied Mathematics, second edition, 2008.

[Fri12] Jürgen Frikel. *Reconstructions in limited angle x-ray tomography: Characterization of classical reconstructions and adapted curvelet sparse regularization*. PhD thesis, Technische Universität München, 2012.

[Fri13] Jürgen Frikel. Sparse regularization in limited angle tomography. *Applied and Computational Harmonic Analysis*, 34(1):117 – 141, 2013.

[Hör71] Lars Hörmander. Fourier integral operators. I. *Acta Mathematica*, 127(1):79–183, 1971.

[Jai89] A.K. Jain. *Fundamentals of digital image processing*. Prentice-Hall information and system sciences series. Prentice Hall, 1989.

[Nat01] Frank Natterer. *The Mathematics of Computerized Tomography*. Society for Industrial and Applied Mathematics, 2001.

[NW01] Frank Natterer and Frank Wübbeling. *Mathematical Methods in Image Reconstruction*. Monographs on Mathematical Modeling and Computation. Society for Industrial and Applied Mathematics, 2001.

[Qui93] Eric T. Quinto. Singularities of the X-Ray Transform and Limited Data Tomography in $\mathbb{R}^2$ and $\mathbb{R}^3$. *SIAM Journal on Mathematical Analysis*, 24(5):1215–1225, 1993.

[Rad17] Johann Radon. Über die Bestimmung von Funktionen durch ihre Integralwerte längs gewisser Mannigfaltigkeiten. *Berichte über die Verhandlungen der Königlich-Sächsischen Gesellschaft der Wissenschaften zu Leipzig. Mathematisch-Physische Klasse 69*, pages 262–277, 1917.

[Rad86] Johann Radon. On the determination of functions from their integral values along certain manifolds. *Medical Imaging, IEEE Transactions on*, 5(4):170 –176, dec. 1986.

[Rag04] Karthik Raghupathy. *Curve tracing and curve detection in images*. PhD thesis, Cornell University, 2004.

[RK96] Alexander G. Ramm and Alexander I. Katsevich. *The Radon Transform and Local Tomography*. CRC Press, 1996.

[WP90] Alan S. Willsky and Jerry L. Prince. Constrained sinogram restoration for limited-angle tomography. *Optical Engineering*, 29(5):535–544, 1990.